

Direct Spectroscopic Confirmation of the Oxygen-Centered Diradical Character of the Tetraoxidorhenium(VII) Cation $[\text{Re}(\text{O})_4]^+$

Mayara da Silva Santos^{+, * [a, b]} Robert Medel^{+, [c]} Simon Kruse,^[b, d] Max Flach,^[a, b]
Olesya S. Abyasova,^[a, b] Martin Timm,^[b] Bernd von Issendorff,^[a] Konstantin Hirsch,^[b]
Vicente Zamudio-Bayer,^[b] Sebastian Riedel,^{* [c]} and J. Tobias Lau^{* [a, b]}

Mononuclear inorganic diradical species are scarce. Here, we confirm, via X-ray absorption spectroscopy in the gas phase combined with computational studies, the oxygen-centered diradical character of the tetraoxidorhenium(VII) cation. A dioxido-superoxido isomer, close in energy to the diradical, is also found, where rhenium appears in its rare oxidation state of +6. Addition of one or two hydrogen atoms to $[\text{Re}_2\text{O}_7]^+$ forms hydroxido ligands, and strongly disfavors isomers with any

oxygen-oxygen bond. This adds spectroscopic characterization of the rhenium oxidation state and the nature of ligands to the known ability of $[\text{Re}_2\text{O}_7]^+$ to perform two consecutive hydrogen-atom abstraction reactions from methane, and demonstrates that pentaatomic $[\text{Re}_2\text{O}_7]^+$ combines a metal center in its highest oxidation state with two oxygen-centered radical ligands in a highly reactive species.

Introduction

Radicals are species that promote the hydrogen-atom transfer (HAT) or abstraction reaction, an important step in several reactions mechanisms.^[1,2] While organic diradicals are vastly investigated,^[2,3] and play important roles as short-lived intermediates in diverse key reactions, such as the cleavage of DNA of tumor cells by enediyne anticancer drugs,^[4] the synthesis of the bioactive natural product neocryptolepine,^[5] and the ozonolysis of organic compounds in the gas phase,^[2,6] much less reports on inorganic metal-oxygen diradicals are available, typically based on spectroscopy, reactivity, or computational studies.^[7–13] In line with the decisive reactivity of such species, it

has been shown that the trinuclear diradical cluster anions $[\text{Sc}_3\text{O}_6]^-$ and $[\text{Al}_3\text{O}_6]^-$ can perform two consecutive hydrogen-atom abstraction reactions from hydrocarbons, forming the dihydrogenated species $[\text{Sc}_3\text{O}_6\text{H}_2]^-$ and $[\text{Al}_3\text{O}_6\text{H}_2]^-$.^[7,13]

Concerning mononuclear oxygen-centered diradical species, only few examples are known. A combination of reactivity and computational studies revealed that the $[\text{Re}_2\text{O}_7]^+$ cation, with a proposed near tetrahedral structure and a triplet ground state with spin density mainly localized at the oxygen ligands, can activate methane by hydrogen-atom transfer.^[12] The main product $[\text{Re}_2\text{O}_7\text{H}]^+$ can further react with a second molecule of methane to yield $[\text{Re}_2\text{O}_7\text{H}_2]^+$.^[12] However, the structure of the $[\text{Re}_2\text{O}_7]^+$ cation has not been directly probed so far, and similar reaction modes were previously attributed to its bis(peroxido) isomer $[\text{Re}(\text{O}_2)_2]^+$ by Beyer et al. They suggested a multi-step mechanism with insertion of the metal center into a C–H bond of methane, followed by hydrogen-atom migration, breaking of an oxygen-oxygen bond, and methyl-radical release to give the intermediate $[\text{Re}(\text{O})(\text{O}_2)(\text{OH})]^+$, which would repeat these steps to finally form $[\text{Re}(\text{O})_2(\text{OH})_2]^+$.^[14] In contrast, photoelectron spectroscopy and computational studies predict that the removal of one electron from the $^1A_1 T_d$ $[\text{Re}(\text{O})_4]^-$ anion would lead to a distorted ($^2A'$ C_3) neutral $[\text{Re}(\text{O})_4]$ molecule.^[15] The electron is removed from the $(1 t_1)^6$ HOMO of $[\text{Re}(\text{O})_4]^-$, which has non-bonding oxygen 2p character, leading to the oxygen-centered radical $[\text{Re}(\text{O})_4]$.^[15] Intuitively, removal of one more electron from the still near-degenerate set of former $(1 t_1)^5$ orbitals would generate the oxygen-centered diradical ion $[\text{Re}(\text{O})_4]^+$. In a similar way, closely-related molecular tetraoxidotungsten(VI), $[\text{W}(\text{O})_4]$ – isoelectronic to $[\text{Re}(\text{O})_4]^+$ – is indicated, by photoelectron spectroscopy combined with computational studies, to have a $^3A_2 D_{2d}$ minimum energy structure, with spin density shared equally over all four oxygen atoms, and its tungsten-oxygen bond lengths of 1.828 Å are

[a] *Physikalisches Institut, Albert-Ludwigs-Universität Freiburg, Freiburg, Germany*

[b] *Abteilung für Hochempfindliche Röntgenspektroskopie, Helmholtz-Zentrum Berlin für Materialien und Energie, Berlin, Germany*


[c] *Institut für Chemie und Biochemie – Anorganische Chemie, Freie Universität Berlin, Berlin, Germany*


[d] *Institut für Physik, Humboldt-Universität zu Berlin, Berlin, Germany*

Correspondence: Mayara da Silva Santos and Prof. Dr. J. Tobias Lau, Physikalisches Institut, Albert-Ludwigs-Universität Freiburg, Hermann-Herder-Straße 3, 79104 Freiburg, Germany.
Email: mayara.da_silva_santos@helmholtz-berlin.de and tobias.lau@helmholtz-berlin.de

Prof. Dr. Sebastian Riedel, Institut für Chemie und Biochemie – Anorganische Chemie, Freie Universität Berlin, Fabeckstraße 34/36, 14195 Berlin, Germany.
Email: s.riedel@fu-berlin.de

[†] *These authors contributed equally to this work.*

 *Supporting Information for this article is available on the WWW under <https://doi.org/10.1002/cmt.202400023>*

 *© 2024 The Author(s). Chemistry - Methods published by Chemistry Europe and Wiley-VCH GmbH. This is an open access article under the terms of the Creative Commons Attribution License, which permits use, distribution and reproduction in any medium, provided the original work is properly cited.*

closer to oxyl rather than oxido ligands, in line with oxygen-centered diradical character.^[8]

Rhenium-containing catalysts are relevant in diverse industrial processes,^[16] including hydrocarbon cracking,^[17] selective hydrogenation,^[18,19] and oxidative transformation of methanol^[20,21] and benzene.^[22] Gas-phase reactivity studies show that $[\text{Re}_2\text{O}_3]^+$ reacts with CH_4 to form $[\text{Re}_2\text{O}_3\text{C}_2\text{H}_2]^+/\text{H}_2$ and $[\text{Re}_2\text{O}_2\text{H}_4]^+/\text{CO}$ products,^[23] while $[\text{Re}_2\text{O}_4]^+$ can activate methane via hydrogen-atom transfer.^[12] Although infrared spectroscopy of gas-phase $[\text{Re}_2\text{O}_3]^{-/0}$ and $[\text{Re}_2\text{O}_4]^{-/0}$; X-ray spectroscopy of bulk ReO_2 and ReO_3 ; photoelectron spectroscopy of bulk ReO_2 and ReO_3 , and of gas-phase $[\text{Re}_2\text{O}_2]^-$, $[\text{Re}_2\text{O}_3]^-$ and $[\text{Re}_2\text{O}_4]^-$ are available,^[15,24–28] direct electronic characterization of oxidorhenium cations is missing so far. Similar to our previous investigation of the oxygen-centered radical character of $[\text{Ru}(\text{O})_4]^+$,^[29] we present here a combined gas-phase X-ray absorption spectroscopy and computational study of $[\text{Re}_n\text{O}_n]^+$ ($n=0-4$) cations, and of the mono and dihydrogenated species $[\text{Re}_n\text{O}_n\text{H}]^+$ and $[\text{Re}_n\text{O}_n\text{H}_2]^+$, to elucidate the oxidation state of the rhenium center and the nature of the oxygen ligands. Experimental and computational details are given in the Methods section and as Supporting Information.

In the oxygen K edge X-ray absorption spectrum of $[\text{Re}_4\text{O}_4]^+$, we identify a clear spectral signature of oxygen-centered holes that persists for the hydrogenated $[\text{Re}_4\text{O}_4\text{H}]^+$ ion but is suppressed for the $[\text{Re}_4\text{O}_4\text{H}_2]^+$ species, just as previously verified for the tetraoxidoruthenium(VIII) cationic oxygen-centered radical $[\text{Ru}_4\text{O}_4]^+$ and its hydrogenated counterpart $[\text{Ru}_4\text{O}_4\text{H}]^+$.^[29] This quenching of the oxygen-centered holes upon dihydrogenation corroborates the theoretical results and reactivity studies by Zhou et al.,^[12] regarding the diradical character of $[\text{Re}_4\text{O}_4]^+$, even though our computational study suggests a close competition of triplet and open-shell singlet states of the tetraoxido $[\text{Re}^{\text{VII}}(\text{O})_4]^+$ isomer with triplet and open-shell singlet states of the dioxido-superoxido $[\text{Re}^{\text{VI}}(\text{O})_2(\text{O}_2)]^+$ isomer. Of these, only the tetraoxido species have an excess of spin density predominantly at the oxygen ligands, *i.e.*, are oxygen-centered diradicals. The coexistence of the nearly-degenerate structural isomers is also indicated experimentally by spectral signatures of oxygen-centered holes and oxygen-oxygen bonds.

Results and Discussion

Structure and Electronic State of $[\text{Re}_4\text{O}_4]^+$

In previous work, combining X-ray absorption spectroscopy with computations, we have verified the oxygen-centered radical character for $[\text{Ru}_4\text{O}_4]^+$, which is spectroscopically indicated by resonant excitation around 526.6 eV at the oxygen K edge. This lowest-energy excitation at the oxygen K edge was assigned to an electronic transition from an oxygen 1s orbital into a singly occupied molecular orbital (SOMO) with non-bonding oxygen 2p character, where $[\text{Ru}_4\text{O}_4]^+$ is assigned to a $[\text{Ru}(\text{O})_4]^+ {}^2\text{B}_2 \text{C}_{2v}$ species, with the spin density of the SOMO

mainly delocalized over two of the four terminal oxygen ligands.

Rhenium, as a group 7 element, can present up to 7 valence electrons for the formation of chemical bonds. Combining rhenium with four oxygen ligands in a mono-cationic species, $[\text{Re}_4\text{O}_4]^+$, results in a two-electron-poor (or one-oxygen-rich) structure, so that oxygen-oxygen bonds or a diradical isomer are feasible. Throughout this work, in molecular formulas without structural information, atoms are separated by commas as, *e.g.*, in $[\text{Re}_4\text{O}_4]^+$. Two isomers of $[\text{Re}_4\text{O}_4]^+$ are discussed in detail along this work, the tetraoxidorhenium(VII) cation $[\text{Re}^{\text{VII}}(\text{O})_4]^+$ and the dioxido-superoxido complex $[\text{Re}^{\text{VI}}(\text{O})_2(\text{O}_2)]^+$. For an intuitive view of these structures, simple two-dimensional valence structural formulas are given in Figure 1, followed by the adopted molecular formulas with structural information.

Similarly to $[\text{Ru}_4\text{O}_4]^+$, for $[\text{Re}_4\text{O}_4]^+$ we again observe a characteristic low-energy transition at 526.4 eV, see experimental spectrum in Figure 2, upper panel. The four energetically lowest isomers and electronic states of $[\text{Re}_4\text{O}_4]^+$ were previously reported by Zhou et al. at CCSD(T,full)//B2GP-PLYP-D3(BJ) level as diradical $[\text{Re}(\text{O})_4]^+$ triplet C_s ; $[\text{Re}(\text{O})_2(\text{O}_2)]^+$ singlet C_2 that, based on the oxygen-oxygen bond length of 1.31 Å, is likely a superoxido complex; $[\text{Re}(\text{O})_4]^+$ singlet C_{3v} ; and a broken-symmetry singlet diradical $[\text{Re}(\text{O})_4]^+ \text{C}_{2v}$ with relative energies of 0, 10, 30 and 54 kJ mol^{-1} , respectively.^[12]

Here, we find related low-energy structures as stable species at the unrestricted BP86 level, with their structures and selected properties summarized in Figure 3. Triplet ($\langle S^2 \rangle = 2.04$) diradical $[\text{Re}^{\text{VII}}(\text{O})_4]^+ {}^3\text{A}_1 \text{D}_{2d}$ is the global minimum, similar to the findings by Zhou et al. for $[\text{Re}(\text{O})_4]^+$ and by Zhai et al. for isoelectronic $[\text{W}(\text{O})_4] {}^3\text{A}_2 \text{D}_{2d}$.^[8] Its spin density is localized over two non-bonding 2p derived orbitals of the four equivalent oxygen atoms and its rhenium-oxygen bond length of 1.758 Å is slightly longer than 1.749 Å for $[\text{Re}^{\text{VII}}(\text{O})_4]^-$ at the same level of theory. In contrast to Zhou et al.,^[12] we find the open-shell broken-symmetry singlet ($\langle S^2 \rangle = 1.06$) diradical species $[\text{Re}^{\text{VII}}(\text{O})_4]^+ {}^1\text{A}_2 \text{C}_{2v}$ with spin-density of opposite sign at different oxygen atoms, at almost the same energy, +3 kJ mol^{-1} at the BP86 level, and -3 kJ mol^{-1} at the CCSD(T)//BP86 level, as the triplet state. Compared to the latter, its molecular symmetry is

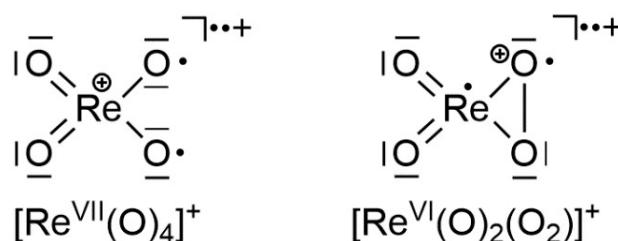


Figure 1. Two-dimensional valence structural and molecular formulas of oxidorhenium cations assigned in this work. Only one resonance form for each isomer is shown. Depending on spin coupling, each structural isomer gives rise to singlet and triplet states, which form the four lowest energy species of $[\text{Re}_4\text{O}_4]^+$. Molecular formulas without structural implications are given throughout the text with elements separated by commas, as in $[\text{Re}_4\text{O}_4]^+$.

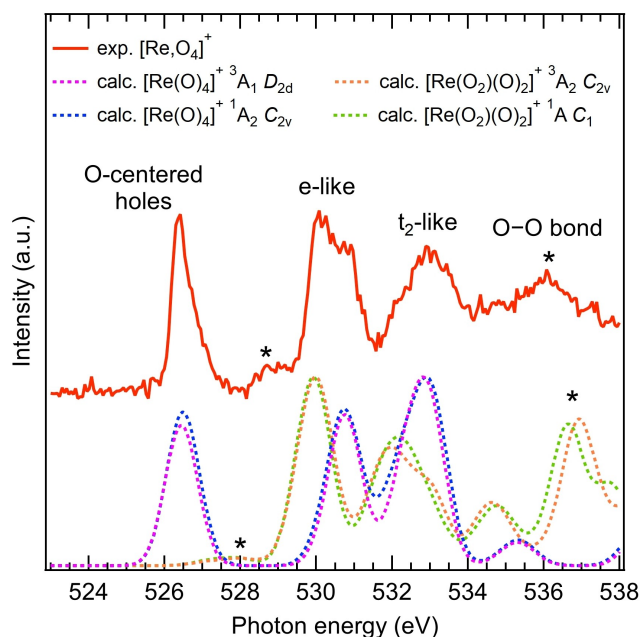


Figure 2. Experimental partial ion yield spectrum (solid red line) at the oxygen K edge of $[\text{Re}(\text{O}_4)]^+$, along with corresponding computational TD-DFT X-ray absorption spectra (dashed lines) for the four lowest energy structures and electronic states $[\text{Re}^{\text{VII}}(\text{O}_4)]^+ {}^3\text{A}_1 D_{2d}$ (magenta), $[\text{Re}^{\text{VII}}(\text{O}_4)]^+ {}^1\text{A}_2 C_{2v}$ (blue), $[\text{Re}^{\text{VI}}(\text{O}_2)(\text{O}_2)]^+ {}^1\text{A} C_1$ (green) and $[\text{Re}^{\text{VI}}(\text{O}_2)(\text{O}_2)]^+ {}^3\text{A}_2 C_{2v}$ (orange). Spectral signatures of oxygen-centered holes in non-bonding p orbitals of the diradical isomer; e- and t_2 -like molecular orbitals of (near-)tetrahedral species; and oxygen-oxygen σ^* orbitals of the dioxido-superoxido isomer are indicated in the figure. Transitions marked by asterisks (*) indicate that dioxido-superoxido complexes are also produced at the experimental conditions.

only slightly reduced from D_{2d} to C_{2v} with almost unchanged bond lengths.

A tendency for radical character is also found for isomers that feature one side-on coordinated O_2 ligand: Closed-shell dioxido-peroxido $[\text{Re}^{\text{VII}}(\text{O}_2)(\text{O}_2)]^+ {}^1\text{A}_1 C_1$ (relative energy of 35 kJ mol^{-1}) is unstable towards relaxation into broken-symmetry ($\langle S^2 \rangle = 0.92$) dioxido-superoxido $[\text{Re}^{\text{VI}}(\text{O}_2)(\text{O}_2)]^+ {}^1\text{A} C_1$ (relative energy of 21 kJ mol^{-1}). Again, differences between the singlet and triplet state of the dioxido-superoxido complex, in terms of energy and structure, are small. Additional CCSD(T) single-point evaluations place all four lowest-energy species within a narrow window of only 8 kJ mol^{-1} (Figure 3). The relative energies are well within the uncertainty of the computational methods and therefore ask for an experimental study. Note that the spin density in the dioxido-superoxido isomer is shared by the rhenium center and the superoxido ligand, different from the lower-energy $[\text{Re}^{\text{VII}}(\text{O}_4)]^+$ diradical isomer, referred to here as oxygen-centered diradical, cf. Figure 3 and Figure S15 for numerical values. Further details on the computational analysis are given as Supporting Information.

The calculated spectra for the four lowest-energy species, identified as singlet and triplet states of diradical or superoxido isomers, respectively, are compared to the experimental spectrum in Figure 2. Furthermore, the molecular orbital diagram of the BP86 global minimum $[\text{Re}^{\text{VII}}(\text{O}_4)]^+ {}^3\text{A}_1 D_{2d}$ is given

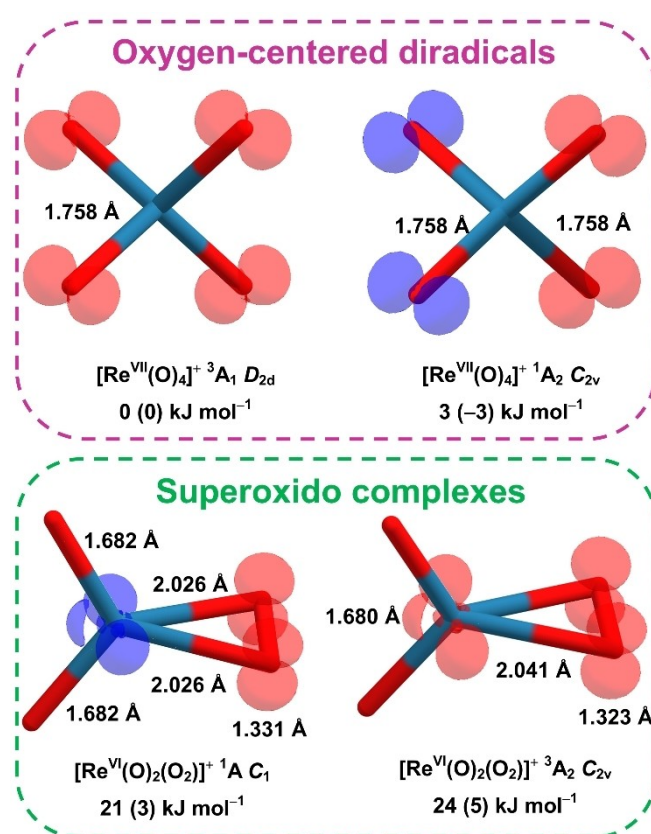


Figure 3. Triplet and singlet states of the lowest-energy isomers of $[\text{Re}(\text{O}_4)]^+$ with their spin densities, bond lengths, electronic states, point groups and relative energies at BP86 level. Relative energies at CCSD(T)/BP86 level are given in parentheses. The $[\text{Re}^{\text{VII}}(\text{O}_4)]^+$ species, with spin density mainly distributed over the terminal oxygen ligands (upper panel) are oxygen-centered diradicals. Oxygen is depicted in red, rhenium in teal. Spin densities are plotted with contour value of 0.05, the red color is used for excess of alpha spin density, and blue for excess of beta spin density.

in Figure 4. The intense pre-edge peak at 526.4 eV is clear evidence for the presence of at least one oxygen-centered diradical species of $[\text{Re}^{\text{VII}}(\text{O}_4)]^+$, as it accounts for the signature of electronic transitions into oxygen-centered holes in non-bonding (n) orbitals.^[29–38] In line with their small differences in geometry and orbital energies (all molecular orbital diagrams are provided in Figures S21–S24), the calculated spectra for the triplet and singlet spin states of $[\text{Re}^{\text{VII}}(\text{O}_4)]^+$ are very similar, allowing no conclusion about preferred parallel or antiparallel spin coupling in the oxygen-centered diradicals. The double-feature between 529.3 and 534.0 eV arises from electronic transitions into e- and t_2 -like molecular orbitals, with π^* and σ^* character, respectively, in (near-)tetrahedral species.^[29,37,39,40] The observed broad signal in the 534 – 538 eV region is not predicted for $[\text{Re}^{\text{VII}}(\text{O}_4)]^+$ but hints at a coexistence of one or more of the close-lying $[\text{Re}^{\text{VI}}(\text{O}_2)(\text{O}_2)]^+$ isomers for which intense σ^* transitions, related to oxygen-oxygen bonds, are expected in this energy range.^[29,39,41] Further support for this hypothesis comes from a weak signal at around 529 eV that might be assigned to excitations into low-lying oxygen-oxygen π^* and rhenium 5d-derived orbitals with small contributions from the oxido ligands. In addition, the width of the 531 eV band is

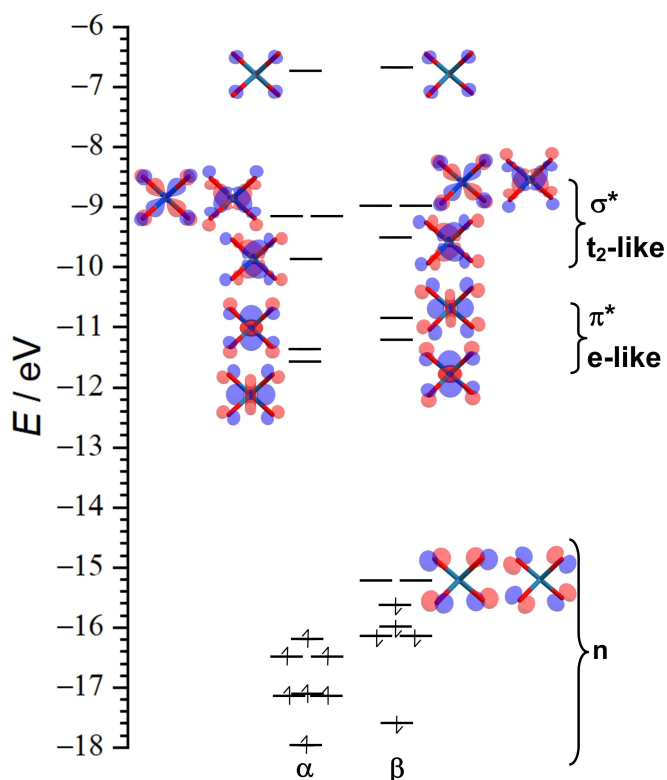


Figure 4. Molecular orbital diagram of diradical $[\text{Re}(\text{O})_4]^+ {}^3A_1 D_{2d}$ calculated at BP86 level. Visualization of occupied non-bonding (n) oxygen p orbitals is omitted for clarity. Unoccupied non-bonding oxygen-centered orbitals are probed by the transition at 526.4 eV in oxygen K edge ion yield spectroscopy, cf. Figures 1 and 5. Oxygen is depicted in red, rhenium in teal. Orbitals are plotted with a contour value of 0.1.

underestimated by the simulation for $[\text{Re}^{\text{VI}}(\text{O})_4]^+$, while the corresponding bands of all other assigned species in this work are reproduced much better. Indeed, for $[\text{Re}^{\text{VI}}(\text{O})_2(\text{O}_2)]^+$ an intense band is predicted at this position that might contribute to the experimental spectrum because of the near degeneracy of isomers.

The rhenium N_3 edge median energies for $[\text{Re}_2\text{O}_7]^+$ and $[\text{Re}_2\text{O}_6]^+$ are similar (Figure S6), confirming a dominant rhenium(VII) species. However, given the large width of the signal and the low signal-to-noise ratio, some contribution of a rhenium(VI) species cannot be ruled out. This is particularly interesting as complexes containing rhenium in the oxidation state +6, with a formal d^1 occupation, are rare.^[42–44] The barrier heights for oxygen-oxygen bond breaking in the ${}^1A_1 C_1$ and ${}^3A_2 C_{2v}$ superoxido isomers, see Supporting Information for potential energy diagram and transition states, are calculated as 133 (133) and 78 (55) kJ mol^{-1} at the triplet and singlet hypersurfaces, respectively. In view of this barrier and of the near-degeneracy of the four lowest-energy species, all within 8 kJ mol^{-1} at the CCSD(T)//BP86 level, it seems plausible that some $[\text{Re}^{\text{VI}}(\text{O})_2(\text{O}_2)]^+$ population might survive the annealing process in the ion source, or cooling in the ion trap.

Diradical Character of $[\text{Re}_2\text{O}_7]^+$ and Oxygen K Edge Spectra of $[\text{Re}_2\text{O}_7\text{H}]^+$ and $[\text{Re}_2\text{O}_7\text{H}_2]^+$

When producing $[\text{Re}_2\text{O}_7]^+$ in the presence of residual water vapor, we observed the appearance of the hydrogenated species $[\text{Re}_2\text{O}_7\text{H}]^+$ and $[\text{Re}_2\text{O}_7\text{H}_2]^+$ in the mass spectrum, as shown in Figure S2. When CH_4 was added to the ion source, the signals of $[\text{Re}_2\text{O}_7\text{H}]^+$ and $[\text{Re}_2\text{O}_7\text{H}_2]^+$ increased significantly, indicative of hydrogen-atom transfer. In the experimental X-ray absorption spectrum of $[\text{Re}_2\text{O}_7\text{H}]^+$ and $[\text{Re}_2\text{O}_7\text{H}_2]^+$ at the oxygen K edge (Figure 5, upper panel) the low-energy transition at 526.4 eV, signature for an oxygen-centered hole, is persistent for $[\text{Re}_2\text{O}_7\text{H}]^+$, but fully quenched for $[\text{Re}_2\text{O}_7\text{H}_2]^+$. Considering that our X-ray spectra are recorded in ion yield mode (cf. Supporting Information), a quantitative correlation between number of unpaired spins and intensity of the low-energy feature is, however, not to be expected. For the oxygen-centered monoradical $[\text{Ru}^{\text{VIII}}(\text{O})_4]^+$, full quenching of the corresponding low-energy transition upon single hydrogenation was observed in similar experimental conditions.^[29]

Hydrogen-atom abstraction from methane or water by $[\text{Re}_2\text{O}_7]^+$ yields $[\text{Re}_2\text{O}_7\text{H}]^+$. Its minimum energy structure has been previously reported as doublet $[\text{Re}^{\text{VI}}(\text{O})_3(\text{OH})]^+ {}^2A'' C_s$ in agreement, we find here $[\text{Re}^{\text{VI}}(\text{O})_2(\text{O})(\text{OH})]^+ {}^2A'' C_s$ with the spin density predominantly residing in a non-bonding orbital with p character of two symmetry-equivalent terminal oxygen atoms. Note that the molecular formula $[\text{Re}(\text{O})_2(\text{O})(\text{OH})]^+$ is adopted here for $[\text{Re}_2\text{O}_7\text{H}]^+$ to consider not only the connectivity but also symmetry and chemical differences of the oxido/oxyl ligands based on the quantum-chemical calculations, see

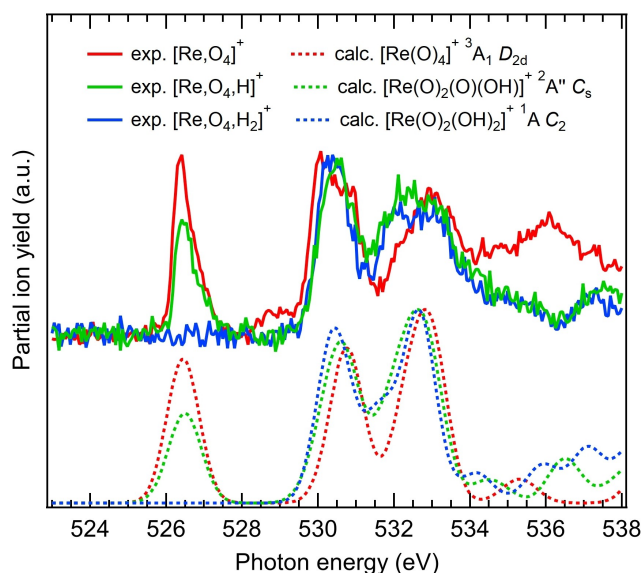


Figure 5. Experimental ion yield spectra at the oxygen K edge (solid lines) of $[\text{Re}_2\text{O}_7]^+$ (red), $[\text{Re}_2\text{O}_7\text{H}]^+$ (green) and $[\text{Re}_2\text{O}_7\text{H}_2]^+$ (blue) along with computational TD-DFT X-ray absorption spectra (dotted lines in corresponding colors) for the respective global minima, $[\text{Re}^{\text{VI}}(\text{O})_4]^+ {}^3A_1 D_{2d}$, $[\text{Re}^{\text{VI}}(\text{O})_2(\text{O})(\text{OH})]^+ {}^2A'' C_s$ and $[\text{Re}^{\text{VI}}(\text{O})_2(\text{OH})_2]^+ {}^1A C_2$. The oxygen-centered character of $[\text{Re}_2\text{O}_7]^+$, indicated by the low-energy transition at 526.4 eV, is only quenched when adding two hydrogen atoms to the molecule, revealing the diradical character of $[\text{Re}_2\text{O}_7]^+$, as well as the monoradical character of monohydrogenated $[\text{Re}_2\text{O}_7\text{H}]^+$.

valence structural formula and calculated structure in Figure 6. The presence of a hydrogen atom is calculated to strongly disfavor isomers with any oxygen-oxygen bonding, cf. Supporting Information, which is supported by the absence of any intense feature in the 534–538 eV region in the computational oxygen K edge spectrum, cf. Figure 5. Formation of $[\text{Re}^{\text{VII}}(\text{O})_2(\text{O})(\text{OH})]^+ \ ^2\text{A}'' \ \text{C}_s$ from $[\text{Re}^{\text{VII}}(\text{O})_4]^+ \ ^3\text{A}_1 \ \text{D}_{2d}$ and methane is calculated to be strongly exothermic by 85 (110) kJ mol^{-1} at BP86 (CCSD(T)//BP86) level, similar to the values of 85 kJ mol^{-1} for $[\text{Os}^{\text{VIII}}(\text{O})_4]^+$ and 73 kJ mol^{-1} for $[\text{Ru}^{\text{VIII}}(\text{O})_4]^+$.^[29,45] In contrast, hydrogen-atom transfer starting from $[\text{Re}^{\text{VI}}(\text{O})_2(\text{O}_2)]^+ \ ^3\text{A}_2 \ \text{C}_{2v}$, as previously suggested to yield the hydroxido-oxido-peroxido species $[\text{Re}^{\text{VI}}(\text{O})(\text{O}_2)(\text{OH})]^+ \ ^2\text{A}' \ \text{C}_s$ is endothermic by 48 (35) kJ mol^{-1} , introducing a sizable barrier in the suggested pathway,^[12] but potentially leading to the possibility of separating the two species in the gas phase by their different reactivity.

A species of the molecular formula $[\text{Re}_4\text{O}_4\text{H}_2]^+$ is a ubiquitous product in the reactions of oxidorhenium cations with hydrogen compounds, apparently because it is thermodynamically strongly favored.^[14] Based on its efficient formation in the (then assumed) simple ligand-exchange reaction $[\text{Re}_4\text{O}_5]^+ + \text{H}_2\text{O} \rightarrow [\text{Re}_4\text{O}_4\text{H}_2]^+ + \text{O}_2$, it was tentatively assigned to the trioxido-aqua complex $[\text{Re}^{\text{VII}}(\text{O})_3(\text{H}_2\text{O})]^+$ rather than to the dihydroxido-dioxido complex $[\text{Re}^{\text{VII}}(\text{O})_2(\text{OH})_2]^+ \ ^1\text{A}_1$.^[14] In contrast, in the same study, the final product of the reaction $[\text{Re}^{\text{V}}(\text{O}_2)_2]^+ + 2 \text{CH}_4 \rightarrow [\text{Re}^{\text{VII}}(\text{O})_2(\text{OH})_2]^+ + 2 \cdot \text{CH}_3$ was formulated as the dihydroxido-dioxido isomer. This reaction with methane was suggested to become possible because of the energy release from the successive breakage of the oxygen-oxygen bonds in the reactant $[\text{Re}^{\text{V}}(\text{O}_2)_2]^+$ and in the intermediate product $[\text{Re}^{\text{VI}}(\text{O})(\text{O})_2(\text{OH})]^+$. In later work this interpretation was computationally challenged: successive hydrogen abstraction from two molecules of methane can also be performed with triplet $[\text{Re}^{\text{VII}}(\text{O})_4]^+$ in a barrier-free and strongly exothermic manner, by

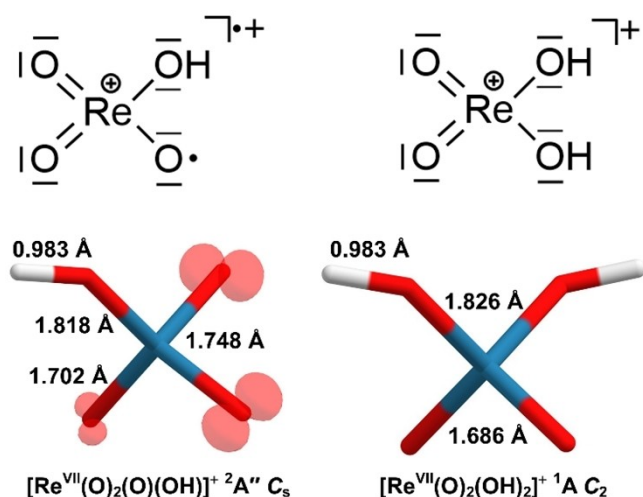


Figure 6. Lowest-energy isomers of $[\text{Re}_4\text{O}_4\text{H}_2]^+$ and $[\text{Re}_4\text{O}_4\text{H}_2]^+$. Valence structural formulas are given in the upper panel, and calculated structures in the lower panel, with spin densities (contour value 0.05), bond lengths, electronic states and point groups. Oxygen is depicted in red, rhenium in teal, hydrogen in white.

115.5 kJ mol^{-1} in the first step and by 157.5 kJ mol^{-1} in the second step, to give $[\text{Re}^{\text{VII}}(\text{O})_2(\text{O})]^+ \ ^{12}$. Here, we confirm $[\text{Re}^{\text{VII}}(\text{O})_2(\text{OH})_2]^+ \ ^1\text{A} \ \text{C}_2$ as the global minimum of $[\text{Re}_4\text{O}_4\text{H}_2]^+$, see valence structural formula and calculated structure in Figure 6. Zero-point-energy corrected hydrogen-atom abstraction from methane by $[\text{Re}^{\text{VI}}(\text{O})_2(\text{O})(\text{OH})]^+ \ ^2\text{A}'' \ \text{C}_s$, forming $[\text{Re}^{\text{VII}}(\text{O})_2(\text{OH})_2]^+ \ ^1\text{A} \ \text{C}_2$, is exothermic by 69 (100) kJ mol^{-1} at BP86 (CCSD(T)//BP86) level in our calculations. More details on the computational studies involving $[\text{Re}_4\text{O}_4\text{H}]^+$ and $[\text{Re}_4\text{O}_4\text{H}_2]^+$ species are given in the Supporting Information.

The calculated oxygen K edge spectra of $[\text{Re}^{\text{VII}}(\text{O})_2(\text{OH})_2]^+ \ ^1\text{A} \ \text{C}_2$ and $[\text{Re}^{\text{VI}}(\text{O})_2(\text{O})(\text{OH})]^+ \ ^2\text{A}'' \ \text{C}_s$ show good agreement with the experimental observations, where the low-energy transition still present in $[\text{Re}_4\text{O}_4\text{H}]^+$ would be the signature of the electronic transition into the singly occupied molecular orbital of oxygen 2p character, shared between all three oxido ligands and shown in Figure 6. Consequently, $[\text{Re}_4\text{O}_4\text{H}]^+$ still shows oxygen-centered radical character, which is only fully quenched for $[\text{Re}_4\text{O}_4\text{H}_2]^+$. These results are further evidence of the diradical character of $[\text{Re}_4\text{O}_4]^+$ and its ability to perform two consecutive hydrogen-atom abstractions from methane. Furthermore, $[\text{Re}_4\text{O}_4\text{H}_2]^+$ could be viewed as the diprotonated closed-shell tetraoxidorhenium(VII) anion, $[\text{Re}(\text{O})_4]^-$, predicted to have a tetrahedral $^1\text{A}_1$ structure.^[46]

Overview of the Complete $[\text{Re}_n\text{O}_n]^+$ ($n = 1-4$) Series

An overview of the oxygen K edge spectra, with extended photon energy range but lower resolution, of the $[\text{Re}_n\text{O}_n]^+$ ($n = 1-4$) series is shown in Figure 7. The main features around 530 eV observed in all spectra are identified as the signature of oxido ligands, as observed in oxidomanganese cations,^[41] oxidorhodium cations,^[39] oxidoruthenium cations,^[29] or oxido-metalates.^[40] Detailed computational analysis of the electronic structures of the $[\text{Re}_n\text{O}_n]^+$ species here studied is given in the Supporting Information.

The electronic ground state of the oxidorhenium cation, $[\text{Re}_n\text{O}_n]^+$, has been suggested as $^3\Delta$,^[47,48] although $^3\Sigma^-$ ^[49] and $^5\Pi$ ^[48] states have also been found. At the computational levels employed here, the global minimum is $[\text{Re}^{\text{III}}\text{O}]^+ \ ^5\Pi \ \text{C}_{\infty v}$ (see Figure S8). Overall, spectroscopic agreement with the three lowest-energy states ($^5\Pi$, $^3\Delta$ and $^3\Sigma^-$) is similar, cf. Figure S9, *i. e.*, for an assignment likely a more elaborate multireference approach will be required in the future.

The global minimum of $[\text{Re}_2\text{O}_2]^+$ has previously been assigned as $[\text{Re}^{\text{V}}(\text{O})_2]^+ \ ^3\text{B}_1 \ \text{C}_{2v}$ ^[48,50] the same as for its lighter congener $[\text{Mn}_2\text{O}_2]^+$,^[41] for which the main features around 530 eV are assigned to electronic transitions into manganese-oxygen π^* molecular orbitals.^[41] Here, we confirm the global minimum $[\text{Re}^{\text{V}}(\text{O})_2]^+ \ ^3\text{B}_1 \ \text{C}_{2v}$ at BP86 level (Figure S10), for which the calculated X-ray absorption spectrum shows good agreement with the experiment.

The most stable isomer of $[\text{Re}_3\text{O}_3]^+$ has been established computationally before as $[\text{Re}^{\text{VII}}(\text{O})_3]^+ \ ^1\text{A}_1 \ \text{C}_{3v}$.^[23,47] This is confirmed here at the BP86 (CCSD(T)//BP86) level but also shown experimentally for the first time, by comparison with the

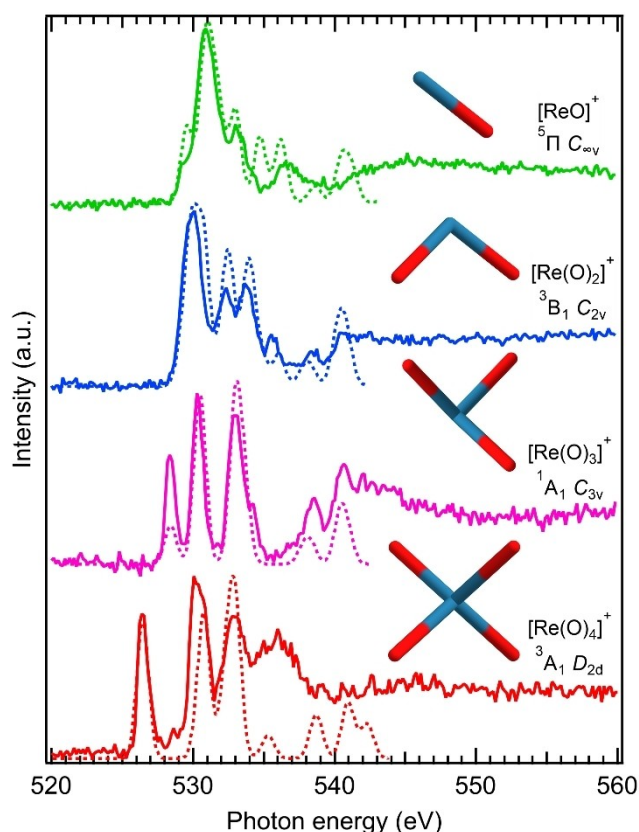


Figure 7. Extended ion yield spectra at the oxygen K edge (solid lines) of the $[\text{Re}(\text{O})_n]^+$ ($n=1-4$) series, and computational TD-DFT X-ray absorption spectra (dotted lines) for the respective global minima, $[\text{ReO}]^+ \ ^5\Pi \ C_{\infty v}$ (green trace), $[\text{Re}(\text{O})_2]^+ \ ^3B_1 \ C_{2v}$ (blue trace), $[\text{Re}^{\text{VI}}(\text{O})_3]^+ \ ^1A_1 \ C_{3v}$ (magenta trace) and $[\text{Re}^{\text{VI}}(\text{O})_4]^+ \ ^3A_1 \ D_{2d}$ (red trace). Higher energy transitions of computational spectra are omitted since agreement between theory and experiment is expected to be poor due to the theoretical approximations employed.^[37] The computational minimum energy structures (oxygen depicted in red, rhenium in teal) of each molecular ion, as well as the electronic state and symmetry, are shown next to the spectra.

oxygen K edge X-ray absorption spectrum (Figure 7). The three prominent oxygen K edge bands are attributed to excitations involving a low-lying π^* LUMO (528.5 eV) as well as the doubly degenerate π^* (530.4 eV) and π^*/σ^* (533.1 eV) LUMO+1 and LUMO+2. For the lighter congener $[\text{Mn}^{\text{VI}}(\text{O})_3]^+ \ ^1A_1 \ C_{3v}$ the gap between LUMO and LUMO+1 is calculated to be smaller, 1.0 eV vs. 1.9 eV at BP86 level, in agreement with the observation that the two low-energy bands overlap much more strongly in the spectrum of $[\text{Mn}^{\text{VI}}(\text{O})_3]^+$.^[41]

As discussed previously, the spectral features observed at the oxygen K edge of $[\text{Re}(\text{O})_4]^+$ account for a low-energy transition into oxygen-centered holes (non-bonding oxygen 2p-derived states) at 526.4 eV; the double feature characteristic of transitions into e- and t_2 -like molecular orbitals, expected at near-tetrahedral symmetry, with π^* (530.1 eV) and σ^* (533.0 eV) character; and the shoulder around 529 eV plus the oxygen-oxygen bond fingerprint in the 534–538 eV region, which are signatures of the dioxido-superoxo isomer, omitted in Fig. 6 for simplicity.

Conclusions

Our gas-phase X-ray absorption spectroscopy study combined with computational studies brings to light a tight energetic competition of tetraoxido diradical and dioxido-superoxo isomers for the global minimum of $[\text{Re}(\text{O})_4]^+$. At the oxygen K edge spectrum, the triplet or open-shell singlet oxygen-centered diradical states $[\text{Re}^{\text{VI}}(\text{O})_4]^+ \ ^3A_1 \ D_{2d}$ and $^1A_2 \ C_{2v}$ are identified by the lowest-energy peak at 526.4 eV, accounted for by oxygen 1s electronic transitions into oxygen-centered holes. Still, the dioxido-superoxo species, $[\text{Re}^{\text{VI}}(\text{O})_2(\text{O}_2)]^+ \ ^1A_1 \ C_1$ and $[\text{Re}^{\text{VI}}(\text{O})_2(\text{O}_2)]^+ \ ^3A_2 \ C_{2v}$, likely coexist as deduced from the spectral feature around 537 eV, which is a signature of an oxygen-oxygen bond, and an additional shoulder around 529 eV, specific to these species. The observation of a rhenium(VI) complex is unusual, and this finding adds to previous $[\text{Re}(\text{O})_4]^+$ investigations that did not account for these isomers. A confirmation of the existence of $[\text{Re}^{\text{VI}}(\text{O})_2(\text{O}_2)]^+$ could be obtained by X-ray circular dichroism, where the spin density over the rhenium center, shown in Figure 3, can be probed directly in future studies. The low-energy transition, indicative of oxygen-centered radical character, is absent for the dihydrogenated species $[\text{Re}^{\text{VI}}(\text{O})_2(\text{OH})_2]^+ \ ^1A_1 \ C_2$, but still present for the monohydrogenated species, $[\text{Re}^{\text{VI}}(\text{O})_2(\text{O})(\text{OH})]^+ \ ^2A'' \ C_s$, confirming an oxygen-centered radical character for the latter. This observation can be viewed as further proof of the diradical behavior of $[\text{Re}(\text{O})_4]^+$ since it takes two hydrogen atoms to fully quench the oxygen-centered holes. Such diradical character of $[\text{Re}(\text{O})_4]^+$ is in line with previous reactivity studies,^[12] but also with the isoelectronic species $[\text{W}(\text{O})_4]$, which prefers fourfold coordination by oxido ligands with delocalized electrons, rather than forming oxygen-oxygen bonds like its lighter congener $[\text{Cr}(\text{O})_4]$.^[8] Similar behaviour is also observed for the lightest congener of $[\text{Re}(\text{O})_4]^+$, $[\text{Mn}(\text{O})_4]^+$, assigned as a superoxido-dioxido manganese(VI) complex.^[41] Two consecutive hydrogen-atom abstractions from methane by $[\text{Re}(\text{O})_4]^+ \ ^3A_1 \ D_{2d}$ are shown to be strongly exothermic, different from the $[\text{Re}(\text{O})_2(\text{O}_2)]^+ \ ^3A_2 \ C_{2v}$ isomer containing a superoxido species. Furthermore, $[\text{Re}(\text{O})_4\text{H}_2]^+$ could also be viewed as diprotonated closed-shell $[\text{Re}(\text{O})_4]^-$,^[51] but no reactivity studies on multiple protonation of $[\text{Re}(\text{O})_4]^-$ have been reported yet. Thus, the full chemistry of rhenium oxides is still to be explored, while electronic, and limited structural, characterization of reactive ionic species becomes available with cryogenic ion trap x-ray spectroscopy.

Methods

Synthesis and Characterization

The $[\text{Re}(\text{O})_n]^+$ ($n=0-4$) molecular ions were produced by argon sputtering of a rhenium target in the presence of oxygen in the buffer gas, which was introduced as a mixture of 1% oxygen in helium 6 N. The cationic species are directed to a quadrupole mass filter, where the ions of interest are selected. The mass selected ions are guided into a linear radio frequency quadrupole ion trap, which is cooled with liquid helium to a typical temperature of 11 K.^[52] The ion trap axis is aligned with the beamline, allowing for

the interaction of the X-rays with the stored and cooled ions. X-ray absorption by the parent ions is followed by an Auger cascade leading to the dissociation of the ions due to Coulomb repulsion and residual internal energy. The ion yield spectrum, representing the X-ray absorption cross section, is obtained by monitoring the product ion intensity, with a time-of-flight mass spectrometer, while scanning the photon energy over an absorption edge. The incident photon energy was scanned in steps of 60 meV with a photon energy bandwidth of 130 meV at the oxygen K edge, or steps of 160 meV steps and photon energy bandwidth of 340 meV for the extended overview spectra (Figure 6), and steps of 120 meV with a photon energy bandwidth of 250 meV at the rhenium N₃ edge. At every photon energy step, an X-ray photoionization-photofragmentation mass spectrum is recorded.

Computational Study

Search for structural isomers and electronic states was initially conducted at the spin-unrestricted BP86^[53,54] level employing the ZORA-def2-TZVP basis set^[55] for oxygen and hydrogen, SARC-ZORA-TZVP for rhenium together with the auxiliary basis SARC/J,^[56,57] in ORCA 5.0.1^[58] (this method is abbreviated throughout the text as BP86). Relative energies were further evaluated with single-point calculations at spin-unrestricted CCSD(T) level employing the aug-cc-pVTZ basis set for oxygen and hydrogen as well as aug-cc-pVTZ-PP for rhenium using Gaussian 16 Rev. A03 (abbreviated as CCSD(T)/BP86). X-ray absorption spectra were calculated using time-dependent density functional theory (TD-DFT) at BP86 level. Calculated spectra were experimentally shifted as stated in the Supporting Information, and all transitions were broadened with a uniform Gaussian profile with a full width at half maximum of 1 eV. Atomic spin populations were calculated in fuzzy partition by Becke^[59] using Multiwfn 3.8(dev).^[60] Exemplary inputs for these methods as well as cartesian coordinates and absolute energies of optimized structures are provided as Supporting Information.

Supporting Information

The authors have cited additional references within the Supporting Information.^[61–71]

Author Contributions

MSS and RM contributed equally to this work. JTL, MSS, and VZB devised the experimental project and prepared the beamtime proposal along with Bvl, KH, MF, MT, OSA, and SK. Bvl, JTL, KH, MT, and VZB designed the experimental setup. Bvl and JTL acquired funding for its realization. MF, MSS, MT, OSA, SK, and VZB performed the experiments and validated their reproducibility. MSS and SK analyzed and interpreted the experimental data under guidance of JTL, KH, and VZB. JTL, KH, and VZB supervised the project. RM performed the computational studies under guidance and supervision of SR. RM analyzed and interpreted the computational results, correlating with the experimental results along with JTL, MSS, SK, SR, and VZB. SR acquired funding for the computational studies. MSS wrote the original draft, with reviewing and editing by JTL, KH, RM, SR, and VZB.

Acknowledgments

Beamtime for this project was granted at the Ion Trap endstation of BESSY II, beamline UE52-PGM, operated by Helmholtz-Zentrum Berlin. This project has received funding from the German Federal Ministry of Education and Research through Grant No. BMBF-05K16VF1. Bvl, JTL, MF, MSS, and OSA acknowledge support by DFG RTG 2717. SR and RM acknowledge funding by ERC Project HighPotOx (818862). Computing time was made available by the High-Performance Computing Center at ZEDAT, Freie Universität Berlin. Open Access funding enabled and organized by Projekt DEAL.

Conflict of Interests

The authors declare no conflict of interest.

Data Availability Statement

The data that support the findings of this study are available from the corresponding author upon reasonable request.

Keywords: gas phase · ground state · radicals · rhenium · X-ray absorption spectroscopy

- [1] Y.-X. Zhao, X.-N. Wu, Z.-C. Wang, S.-G. He, X.-L. Ding, *Chem. Commun.* **2010**, 46, 1736–1738.
- [2] T. Stuyver, B. Chen, T. Zeng, P. Geerlings, F. De Proft, R. Hoffmann, *Chem. Rev.* **2019**, 119, 11291–11351.
- [3] G. Cilento, W. Adam, *Free Radical Biol. Med.* **1995**, 19, 103–114.
- [4] E. Kraka, D. Cremer, *J. Am. Chem. Soc.* **2000**, 122, 8245–8264.
- [5] A. B. J. Bracca, D. A. Heredia, E. L. Larghi, T. S. Kaufman, *Eur. J. Org. Chem.* **2014**, 2014, 7979–8003.
- [6] D. Johnson, G. Marston, *Chem. Soc. Rev.* **2008**, 37, 699–716.
- [7] L.-H. Tian, T.-M. Ma, X.-N. Li, S.-G. He, *Dalton Trans.* **2013**, 42, 11205–11211.
- [8] H.-J. Zhai, B. Kiran, L.-F. Cui, X. Li, D. A. Dixon, L.-S. Wang, *J. Am. Chem. Soc.* **2004**, 126, 16134–16141.
- [9] E. Janssens, G. Santambrogio, M. Brümmer, L. Wöste, P. Lievens, J. Sauer, G. Meijer, K. R. Asmis, *Phys. Rev. Lett.* **2006**, 96, 233401.
- [10] H.-J. Zhai, W.-J. Chen, S.-J. Lin, X. Huang, L.-S. Wang, *J. Phys. Chem. A* **2013**, 117, 1042–1052.
- [11] H.-J. Zhai, X.-H. Zhang, W.-J. Chen, X. Huang, L.-S. Wang, *J. Am. Chem. Soc.* **2011**, 133, 3085–3094.
- [12] S. Zhou, M. Schlangen, H. Schwarz, *Chem. Eur. J.* **2017**, 23, 17469–17472.
- [13] Y.-X. Zhao, J.-Y. Yuan, X.-L. Ding, S.-G. He, W.-J. Zheng, *Phys. Chem. Chem. Phys.* **2011**, 13, 10084–10090.
- [14] M. K. Beyer, C. B. Berg, V. E. Bondybey, *Phys. Chem. Chem. Phys.* **2001**, 3, 1840–1847.
- [15] W.-J. Chen, H.-J. Zhai, X. Huang, L.-S. Wang, *Chem. Phys. Lett.* **2011**, 512, 49–53.
- [16] V. G. Kessler, G. A. Seisenbaeva, *Minerals* **2012**, 2, 244–257.
- [17] N. Escalona, M. Vrinat, D. Laurenti, F. J. Gil Llambias, *Appl. Catal. Gen.* **2007**, 322, 113–120.
- [18] K. Liu, J. Pritchard, L. Lu, R. van Putten, M. W. G. M. Verhoeven, M. Schmitkamp, X. Huang, L. Lefort, C. J. Kiely, E. J. M. Hensen, E. A. Pidko, *Chem. Commun.* **2017**, 53, 9761–9764.
- [19] T. Toyao, K. Wei Ting, S. M. A. Hakim Siddiki, A. S. Touchy, W. Onodera, Z. Maeno, H. Ariga-Miwa, Y. Kanda, K. Asakura, K. Shimizu, *Catal. Sci. Technol.* **2019**, 9, 5413–5424.
- [20] A. S. Y. Chan, W. Chen, H. Wang, J. E. Rowe, T. E. Madey, *J. Phys. Chem. B* **2004**, 108, 14643–14651.
- [21] Y. Yuan, T. Shido, Y. Iwasawa, *Chem. Commun.* **2000**, 1421–1422.

- [22] T. Kusakari, T. Sasaki, Y. Iwasawa, *Chem. Commun.* **2004**, 0, 992–993.
- [23] S. Zhou, X. Sun, L. Yue, M. Schlagen, *Int. J. Mass Spectrom.* **2018**, *434*, 240–245.
- [24] J. Purans, A. Kuzmin, P. Parent, C. Laffon, *Phys. Condens. Matter* **1999**, *259–261*, 1157–1158.
- [25] A. Tougeri, S. Cristol, E. Berrier, V. Briois, C. La Fontaine, F. Villain, Y. Joly, *Phys. Rev. B* **2012**, *85*, 125136.
- [26] E. Brockawik, J. Haber, L. Ungier, *J. Phys. Chem. Solids* **1981**, *42*, 203–208.
- [27] A. Pramann, K. Rademann, *Chem. Phys. Lett.* **2001**, *343*, 99–104.
- [28] M. Zhou, A. Citra, B. Liang, L. Andrews, *J. Phys. Chem. A* **2000**, *104*, 3457–3465.
- [29] M. da Silva Santos, R. Medel, M. Flach, O. S. Ablyasova, M. Timm, B. von Issendorff, K. Hirsch, V. Zamudio-Bayer, S. Riedel, J. T. Lau, *ChemPhysChem* **2023**, *24*, e202300390.
- [30] R. A. House, U. Maitra, M. A. Pérez-Osorio, J. G. Lozano, L. Jin, J. W. Somerville, L. C. Duda, A. Nag, A. Walters, K. J. Zhou, M. R. Roberts, P. G. Bruce, *Nature* **2020**, *577*, 502–508.
- [31] A. Braun, K. Sivula, D. K. Bora, J. Zhu, L. Zhang, M. Grätzel, J. Guo, E. C. Constable, *J. Phys. Chem. C* **2012**, *116*, 16870–16875.
- [32] Y. Uemura, A. S. M. Ismail, S. H. Park, S. Kwon, M. Kim, H. Elnaggar, F. Frati, H. Wadati, Y. Hirata, Y. Zhang, K. Yamagami, S. Yamamoto, I. Matsuda, U. Halisdemir, G. Koster, C. Milne, M. Ammann, B. M. Weckhuysen, F. M. F. de Groot, *J. Phys. Chem. Lett.* **2022**, *13*, 4207–4214.
- [33] V. Pfeifer, T. E. Jones, J. J. V. Vélez, C. Massué, M. T. Greiner, R. Arrigo, D. Teschner, F. Girgsdies, M. Scherzer, J. Allan, M. Hashagen, G. Weinberg, S. Piccinin, M. Hävecker, A. Knop-Gericke, R. Schlögl, *Phys. Chem. Chem. Phys.* **2016**, *18*, 2292–2296.
- [34] C. T. Chen, F. Sette, Y. Ma, M. S. Hybertsen, E. B. Stechel, W. M. C. Foulkes, M. Schulter, S.-W. Cheong, A. S. Cooper, L. W. Rupp, B. Batlogg, Y. L. Soo, Z. H. Ming, A. Krol, Y. H. Kao, *Phys. Rev. Lett.* **1991**, *66*, 104–107.
- [35] Z. H. Loh, G. Doumy, C. Arnold, L. Kjellsson, S. H. Southworth, A. Al Haddad, Y. Kumagai, M. F. Tu, P. J. Ho, A. M. March, R. D. Schaller, M. S. Bin Mohd Yusof, T. Debnath, M. Simon, R. Welsch, L. Inhester, K. Khalili, K. Nanda, A. I. Krylov, S. Moeller, G. Coslovich, J. Koralek, M. P. Minitti, W. F. Schlotter, J. E. Rubensson, R. Santra, L. Young, *Science* **2020**, *367*, 179–182.
- [36] E. J. Mele, J. J. Ritsko, *Phys. Rev. Lett.* **1979**, *43*, 68–71.
- [37] F. Frati, M. O. J. Y. Hunault, F. M. F. De Groot, *Chem. Rev.* **2020**, *120*, 4056–4110.
- [38] T. J. A. Wolf, R. H. Myhre, J. P. Cryan, S. Coriani, R. J. Squibb, A. Battistoni, N. Berrah, C. Bostedt, P. Bucksbaum, G. Coslovich, R. Feifel, K. J. Gaffney, J. Grilj, T. J. Martinez, S. Miyabe, S. P. Moeller, M. Mucke, A. Natan, R. Obaid, T. Osipov, O. Plekan, S. Wang, H. Koch, M. Gühr, *Nat. Commun.* **2017**, *8*, 29.
- [39] M. da Silva Santos, T. Stüker, M. Flach, O. S. Ablyasova, M. Timm, B. von Issendorff, K. Hirsch, V. Zamudio-Bayer, S. Riedel, J. T. Lau, *Angew. Chem. Int. Ed.* **2022**, *61*, e202207688.
- [40] S. G. Minasian, J. M. Keith, E. R. Batista, K. S. Boland, J. A. Bradley, S. R. Daly, S. A. Kozimor, W. W. Lukens, R. L. Martin, D. Nordlund, G. T. Seidler, D. K. Shuh, D. Sokaras, T. Tyliczszak, G. L. Wagner, T.-C. Weng, P. Yang, *J. Am. Chem. Soc.* **2013**, *135*, 1864–1871.
- [41] M. G. Delcey, R. Lindblad, M. Timm, C. Bülow, V. Zamudio-Bayer, B. von Issendorff, J. T. Lau, M. Lundberg, *Phys. Chem. Chem. Phys.* **2022**, *24*, 3598–3610.
- [42] J. Mukiza, T. I. A. Gerber, E. Hosten, A. S. Ogunlaja, F. Taherkhani, M. Amini, M. Nahali, *Inorg. Chem. Commun.* **2015**, *51*, 83–86.
- [43] D. D. DuMez, J. M. Mayer, *Inorg. Chem.* **1998**, *37*, 445–453.
- [44] J. I. van der Vlugt, *Chem. Eur. J.* **2019**, *25*, 2651–2662.
- [45] G. Zhang, S. Li, Y. Jiang, *Organometallics* **2004**, *23*, 3656–3667.
- [46] J. Gancheff, C. Kremer, E. Kremer, O. N. Ventura, *J. Mol. Struct.* **2002**, *580*, 107–116.
- [47] M. Beyer, C. Berg, S. Joos, U. Achatz, W. Hieringer, G. Niedner-Schatteburg, V. E. Bondybey, *Int. J. Mass Spectrom.* **1999**, *185–187*, 625–638.
- [48] P. B. Armentrout, *J. Chem. Phys.* **2013**, *139*, 084305.
- [49] C. Yao, W. Guan, P. Song, Z. M. Su, J. D. Feng, L. K. Yan, Z. J. Wu, *Theor. Chem. Acc.* **2007**, *117*, 115–122.
- [50] J. Kim, R. M. Cox, P. B. Armentrout, *Phys. Chem. Chem. Phys.* **2020**, *22*, 3191–3203.
- [51] J. Jian, E. Varathan, T. Cheisson, T. Jian, W. W. Lukens, R. L. Davis, E. J. Schelter, G. Schreckenbach, J. K. Gibson, *Phys. Chem. Chem. Phys.* **2020**, *22*, 12403–12411.
- [52] A. Langenberg, K. Hirsch, A. Ławicki, V. Zamudio-Bayer, M. Niemeyer, P. Chmiela, B. Langbehn, A. Terasaki, B. v. Issendorff, J. T. Lau, *Phys. Rev. B* **2014**, *90*, 184420.
- [53] A. D. Becke, *J. Chem. Phys.* **1993**, *98*, 1372–1377.
- [54] J. P. Perdew, *Phys. Rev. B* **1986**, *34*, 7406.
- [55] F. Weigend, R. Ahlrichs, *Phys. Chem. Chem. Phys.* **2005**, *7*, 3297–3305.
- [56] F. Weigend, *Phys. Chem. Chem. Phys.* **2006**, *8*, 1057–1065.
- [57] J. D. Rolfes, F. Neese, D. A. Pantazis, *J. Comput. Chem.* **2020**, *41*, 1842–1849.
- [58] F. Neese, *WIREs Comput. Mol. Sci.* **2022**, *12*, e1606.
- [59] A. D. Becke, *Phys. Rev. A* **1988**, *38*, 3098–3100.
- [60] T. Lu, F. Chen, *J. Comput. Chem.* **2012**, *33*, 580–592.
- [61] K. Hirsch, J. T. Lau, P. Klar, A. Langenberg, J. Probst, J. Rittmann, M. Vogel, V. Zamudio-Bayer, T. Möller, B. von Issendorff, *J. Phys. B* **2009**, *42*, 154029.
- [62] J. J. Melko, S. G. Ard, T. Lê, G. S. Miller, O. Martinez, N. S. Shuman, A. A. Viggiano, *J. Phys. Chem. A* **2017**, *121*, 24–30.
- [63] G. Van Der Laan, I. W. Kirkman, *J. Phys. Condens. Matter* **1992**, *4*, 4189–4204.
- [64] H. Tan, J. Verbeeck, A. Abakumov, G. Van Tendeloo, *Ultramicroscopy* **2012**, *116*, 24–33.
- [65] O. S. Ablyasova, M. Guo, V. Zamudio-Bayer, M. Kubin, T. Gitzinger, M. da Silva Santos, M. Flach, M. Timm, M. Lundberg, J. T. Lau, K. Hirsch, *J. Phys. Chem. A* **2023**, *127*, 7121–7131.
- [66] F. D. Groot, *Coord. Chem. Rev.* **2005**, *249*, 31–63.
- [67] J. Chen, *Catal. Today* **1998**, *43*, 147–158.
- [68] M. Flach, K. Hirsch, M. Timm, O. S. Ablyasova, M. da S Santos, M. Kubin, C. Bülow, T. Gitzinger, B. von Issendorff, J. T. Lau, V. Zamudio-Bayer, *Phys. Chem. Chem. Phys.* **2022**, *24*, 19890–19894.
- [69] V. Brites, K. Franzreb, J. N. Harvey, S. G. Sayres, M. W. Ross, D. E. Blumling, A. W. Castleman, M. Hochlaf, *Phys. Chem. Chem. Phys.* **2011**, *13*, 15233–15243.
- [70] R. S. Mulliken, *J. Chem. Phys.* **1955**, *23*, 1997–2011.
- [71] F. Neese, *Coord. Chem. Rev.* **2009**, *253*, 526–563.

Manuscript received: July 11, 2024

Version of record online: October 25, 2024